Journal of Quantitative Spectroscopy & Radiative Transfer 166 (2015) 23–29

Contents lists available at ScienceDirect

Journal of Quantitative Spectroscopy & Radiative Transfer

journal homepage: www.elsevier.com/locate/jqsrt

Diode laser cavity ring-down spectroscopy for in situ measurement of NO_3 radical in ambient air

Dan Wang [a], Renzhi Hu [a], Pinhua Xie [a,b,*], Jianguo Liu [a], Wenqing Liu [a], Min Qin [a], Liuyi Ling [c], Yi Zeng [a], Hao Chen [a], XingBiao Xing [a], Guoliang Zhu [a], Jun Wu [a], Jun Duan [a], Xue Lu [a], Lanlan Shen [a]

[a] Anhui Institute of Optics and Fine Mechanics, Key Laboratory of Environmental Optics and Technology, Chinese Academy of Sciences, Hefei 230031, China
[b] School of Environmental Science and Optoelectronic Technology, University of Science and Technology of China, Hefei 230026, China
[c] Institute of Electric and Information Technology, Anhui University of Science and Technology, Huainan 232001, China

ARTICLE INFO

Article history:
Received 10 February 2015
Received in revised form
7 June 2015
Accepted 13 July 2015
Available online 20 July 2015

Keywords:
NO_3 radical
Cavity ring-down spectroscopy (CRDS)
Atmospheric monitoring
Diode laser

ABSTRACT

A cavity ring-down spectroscopy (CRDS) instrument for measuring atmospheric NO_3 radical developed in our laboratory is presented in detail. Light from a red laser diode (661.85 nm) is coupled on-axis into an optical cavity formed by a pair of high-reflectivity mirrors ($R \geq 99.9985\%$) to achieve an effective absorption path length of approximately 20 km. The detection limit of the NO_3 radical determined by Allan variance for the field observation with high particles is approximately 3.2 pptv (2σ, 10 s). The transmission efficiency of the NO_3 radical in the system is calibrated, including the filter loss and surface loss. Moreover, measurable interferences from NO_2, O_3 and water vapor are also discussed. Considering the influence of inlet transmission efficiency and other factors, the instrument accuracy for NO_3 radical measurement is approximately $\pm 8\%$ (1σ).

The measurement of NO_3 radical was performed at a suburb site in Beijing under the situation of high particles concentration ($PM_{2.5}$ approximately several tens to 150 $\mu g/m^3$) from October 26 to November 11, 2014. The NO_3 radical concentration during the period is relatively low with the maximum value of 38 pptv. The observation results on October 29, combining NO_2, O_3 and NO data, are briefly analyzed. The experimental results demonstrate that this compact CRDS instrument has the potential for NO_3 radical measurements in the field with high particles.

1. Introduction

Nitrate radical (NO_3) is a significant nocturnal trace gas in the atmosphere [1], its oxidative capacity in the night is comparable with that of diurnal OH radical [2,3]. NO_3 radical contributes to the oxidation of hydrocarbons [4] and organic sulfur species [5], as well as the conversion of nitrogen oxides to nitric acid [6] at night. NO_3 radical is formed by the reaction of O_3 with NO_2, and it reacts with NO_2 to form N_2O_5, which is in a temperature dependent equilibrium with NO_3 radical.

$$NO_2 + O_3 \rightarrow NO_3 + O_2$$

$$NO_3 + NO_2 \leftrightarrow N_2O_5 \qquad (2)$$

NO_3 radical is rapidly photodissociated during daytime [1]. Thus, a mass of NO_3 radical can only be accumulated at night. Another key loss process is the reaction of NO_3

* Corresponding author.
E-mail address: phxie@aiofm.ac.cn (P. Xie).

http://dx.doi.org/10.1016/j.jqsrt.2015.07.005

radical with NO as follows:

$$NO_3 + NO \rightarrow 2NO_2 \quad (3)$$

With a rate constant of k (298 K)=2.6 × 10^{-11} cm^3 $molecule^{-1}$ s^{-1} [7], the reaction significantly limits the NO_3 lifetime in the presence of NO. Given the importance of NO_3 radical in the nocturnal chemical process, accurate measurement of its concentration in the atmosphere has become an essential topic in current research.

Previous observations of NO_3 radical are primarily performed by differential optical absorption spectroscopy (DOAS) [8–10]. Long-path DOAS (LP-DOAS) detects the average NO_3 radical concentration over a multi-kilometer path, with the time resolution on the order of the minutes [11–15]. In the recent years, chemical ionization mass spectrometry (CIMS), cavity enhanced absorption spectroscopy (CEAS), and cavity ring-down spectroscopy (CRDS) have been developed to detect NO_3 radical [16–19]. CIMS is a non-optical method that has been applied to detect the sum of NO_3 and N_2O_5 by their reactions with I^- [20,21]. In contrast to CIMS, CEAS and CRDS are both optical methods that use high-reflectivity mirrors to achieve a long effective path length. With the development of CEAS, it has been applied to detect NO_3 radical in the chamber and the field [22,23], and the detection limits can reach 0.25–8 pptv in integration times of seconds to minutes [17,24,25]. CRDS was presented by Brown et al. to measure NO_3 and N_2O_5 in 2001 [26] and has since been gradually developed [27–29]. Recently, CRDS has been developed for aircraft simultaneous measurements of NO_3, N_2O_5, NO, NO_2 and O_3 with the NO_3 detection limit of 3 pptv (1 s) [16]. In addition, Ayers et al. and Schuster et al. have also used off-axis CRDS technique for the measurement of NO_3 radical with the higher sensitivity of 1.4–2 pptv (5 s) [30,31]. As a high sensitivity technique for direct absorption measurement, CRDS also has the advantages of smaller power consumption, size, and weight. Thus the CRDS instruments for measurement of NO_3 radical can be deployed on several platforms, such as ground sites [30], tall towers [32], ships [33], as well as aircrafts [16]. The ambient NO_3 measurement in China is very scarce, only LP-DOAS technique was used [14,15]. Different from LP-DOAS detecting the average NO_3 radical concentration along the light path, CRDS is one kind of point sampling instrument that can monitor in-situ local NO_3 radical. At present, the above described CRDS instrument for NO_3 radical detection is applied in relatively clean air mass [34]. To our knowledge, it is a challenge for CRDS instrument to measure NO_3 radical under the situation of high particles concentration.

We have developed a CRDS instrument for NO_3 radical detection in ambient air. The setup of the instrument, the calibration for NO_3 radical and the field observations are described. A series of laboratory tests have been carried out to quantify the surface loss of NO_3 radical and the inlet filter loss of NO_3 radical of the CRDS system, especially for the filter to remove the aerosol in the ambient air. Moreover, CRDS instrument was used for the ambient NO_3 radical measurement in the suburb of Beijing, China under the situation of high particles concentration ($PM_{2.5}$ approximately several tens to 150 μg/m^3).

2. CRDS and instrument description

2.1. Cavity ring-down spectroscopy

CRDS is a spectroscopy technique to detect atmospheric trace gases that rely on measurements of the attenuation rate [35–38]. The absorber concentration [A] is calculated by the ring-down time constants (τ) and (τ_0), which represent the presence and absence of the absorber in the cavity, respectively

$$[A] = \frac{R_L}{c\sigma}\left(\frac{1}{\tau} - \frac{1}{\tau_0}\right) \quad (4)$$

where σ is the absorption cross section for A, c is the speed of light, and R_L is the ratio of the total cavity length to the length of cavity containing the NO_3 radical. Here [A] is the number density and presented in the form of volume mixing ratio by the formula conversion in the whole article.

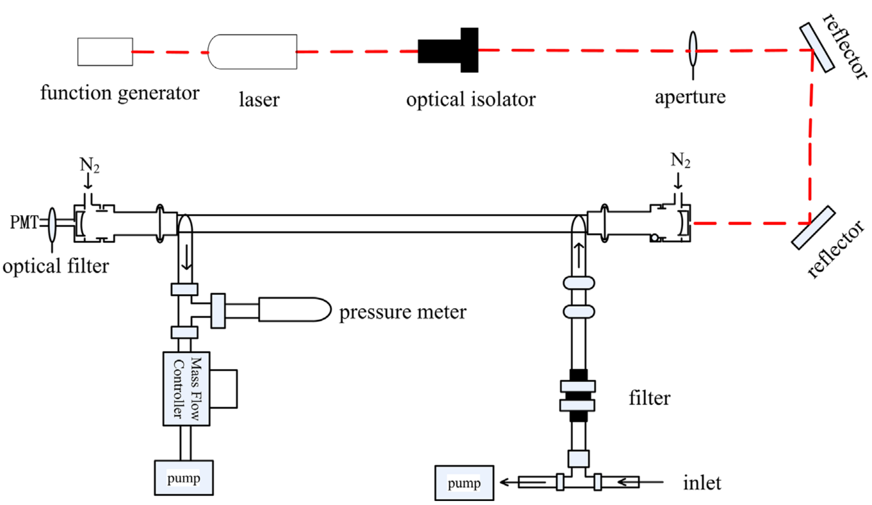

Fig. 1. Experimental layout of the pulsed CRDS instrument for NO_3 radical detection.

2.2. CRDS instrument description

The schematic of the CRDS system used for measuring NO_3 radical is shown in Fig. 1. Light is provided by an external modulation diode laser (line width 0.3 nm) with an optical output of approximately 120 mw. The laser is pulsed through the function generator (DG1022, RIGOL), and the laser output is modulated with a square-wave signal at a repetition rate of 150 Hz. The center wavelength of the diode laser is 661.85 nm (IQμ, Power Technology Inc.), closer to the NO_3 absorption peak of 662 nm.

The laser light is propagated through an optical isolator (IO-3D-660-VLP, Thorlabs) placed in front of the laser to reduce optical feedback to the diode laser. The light is then coupled into the optical cavity (curvature, 1 m; distance, 76 cm), which is formed by a pair of high-reflectivity ($R \geq 99.9985\%$) mirrors. The cavity is made of PFA tube (3/8 in. diameter) and fixed by an aluminum wedge. A small flow of dry N_2 (0.1–0.2 SLPM) is introduced directly to maintain the cleanliness of the mirrors. The light transmitted through the back mirror passes through an optical filter centered at 662 nm (bandwidth for 10 nm), and then is detected by a photomultiplier tube (PMT) (Hamamatsu H10721-20). The optical filter prevents the stray light at other wavelengths from influencing the measurement. Signals from the PMT are digitized using oscilloscope card (PCI 6132, 2.5 MS s^{-1}), that is controlled by the LabVIEW program to acquire the ring-down traces. Individual decay profiles of 1500 are co-added, and then averaged to achieve a higher signal to noise ratio. An example cavity decay trace is shown in Fig. 2.

Considering the standard deviation of fitting results of the Levenberg–Marquardt (LM) algorithm, the best record length is approximately (5–7)τ [39,40]. Thus, the range of the fitting includes approximately 340 μs. The ring-down time of the system is approximately 68.00 μs (τ_0) and the calculated effective path length is approximately 20 km.

The inlet system consists of two parts: an aerosol filter and a flow system. The flow system is composed of PFA tubings (3/8 in. inner diameter or 1/4 in. outer diameter) and accessories. The length from the inlet to the midpoint of the ring-down cell is approximately 75 cm. To remove the atmospheric NO_3 radical (> 99%), approximately 35 ppbv of NO is added into the flow system before the filtering process. In this case, τ_0 (the absence of the absorber in the cavity) is measured. The stream of NO contains a small amount of NO_2 (< 1%), which hardly affects the measurement of τ_0 [27]. The injected NO may react with O_3 in the atmosphere at a rate constant of $k = 1.80 \times 10^{-14}$ cm^3 $molecule^{-1}$ s^{-1} [7] that is smaller (factor 3) than the rate constant of the reaction of NO with NO_3. Therefore, atmospheric O_3 barely impacts the measurement of τ_0.

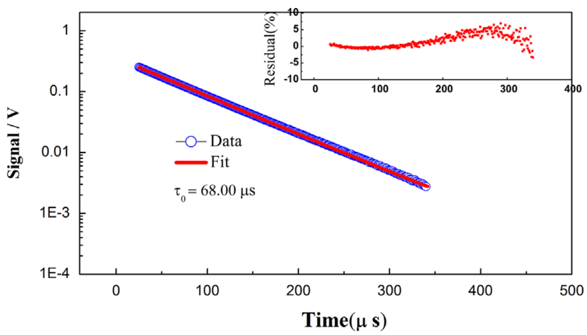

Fig. 2. Cavity ring-down signal and fitting. The small figure in the upper right corner is the fitting residual.

The sampled air passes through a Teflon filter holder (Cole–Parmer R-06621-40) containing a 2 μm pore size Teflon membrane filter (Pall Corp.). The Teflon membrane filter is added to remove the atmospheric particles that may affect the measurement of NO_3 radical in the optical cavity. Nevertheless, removing the particles using the Teflon membrane can also result in additional loss of NO_3 radical. The calibration of NO_3 radical loss in the system is described in detail in the following part.

3. Calibration

NO_3 radical is a reactive species; hence, its loss in the inlet system must be calibrated to obtain accurate concentrations of NO_3 radical. Measurements of surface loss and membrane filter loss are carried out using synthetic N_2O_5 produced by a standard method [41]. Calibration samples of N_2O_5 or NO_3 radical are generated by passing a small flow of N_2 over a sample of solid N_2O_5 stored at −78 °C (dry ice). The samples are diluted in N_2 and pass through an additional heater to convert N_2O_5 to NO_3 radical. The additional heater is constructed of 1/4 in. outer diameter PFA tube (approximately 45 cm) and the surface of tube is heated to 80 °C (controlled by temperature controller, the precision of approximately ±1 °C).

3.1. Surface loss

The surface loss of NO_3 radical through the PFA tubing with 3/8 in. inner diameter is measured in the laboratory using a heated N_2O_5 source. The transmission is fitted to a straight line as a function of the residence time [27]. Fig. 3 shows the measurement of the NO_3 radical transmission efficiency through the tubing plus the Teflon filter holder (no Teflon membrane filter in the system). The loss through the Teflon filter holder is a constant [28], which acts as a point source loss for NO_3 radical and is introduced into the concentration equations. Variation of the residence time (0.4–2 s) is obtained by changing the flow rates. For our current system, when the loss through the holder is 9 ± 4%, the loss rate coefficient $k = 0.19 \pm 0.02$ s^{-1} is obtained by a linear fit that depends on the residence time. Every set of graphic symbols represents a separate measurement and the time of each measurement is short (less than 2 min). During each measurement, the output NO_3 radical concentration of the heated N_2O_5 source can be considered as relatively stable.

3.2. Inlet filter transmission

For reducing Mie scattering interference, the filter is added in the inlet system to remove the aerosol. The Teflon

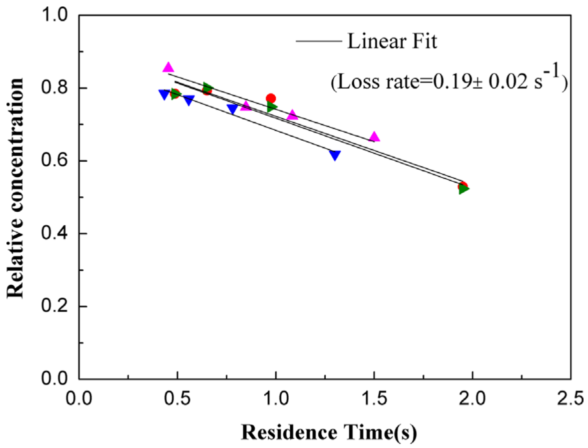

Fig. 3. Surface loss of NO_3 radical through the PFA tubing with 3/8 in. inner diameter is measured in the laboratory. The residence time represents the time from the tubing inlet to the center of the cavity. The residence time is varied by changing the flow rates. By correction and calculation, the ratio of the measured NO_3 radical concentration to the original NO_3 radical concentration (no loss concentration before entering into the system) is obtained. The ratio represents relative concentration. The solid line is the first-order linear fits of the surface loss. The average first-order loss rate is $k=0.19\pm0.02\ s^{-1}$.

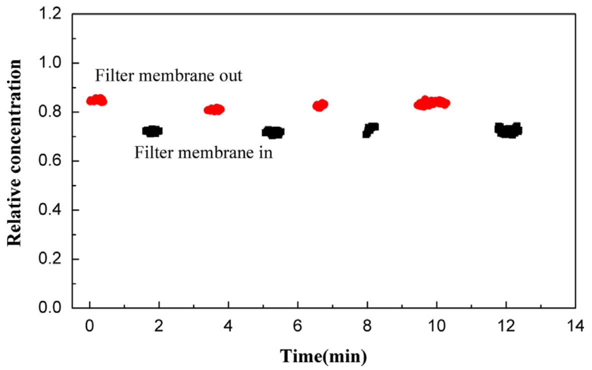

Fig. 4. The transmission efficiency of NO_3 radical through the Teflon membrane filter is measured in the laboratory. The Teflon membrane filter is used about 2 h for the field experiment at 5 SLPM flow rate. The figure shows the overall transmission efficiency of the system after inserting and removing filter membrane, considering filter hold loss and surface loss. The abscissa is the time of the Teflon membrane filter transmission measurement. The relative concentration is the ratio of the measured NO_3 radical concentration to the original NO_3 radical concentration (no loss concentration before entering into the system).

membrane filter is changed every 1–2 h during the field observation to reduce loss in the inlet system. Under the situation of high particles concentration ($PM_{2.5}$ approximately 70 μg/m^3, PM_{10} about 150 μg/m^3), the transmission efficiencies of Teflon membrane filter may vary over time. To obtain accurate concentration of NO_3 radical under the situation of high particles concentration, the transmission efficiency of the new membrane filter and used membrane filter is calibrated. Based on the measuring surface loss, the membrane filter (used for about 2 h during the field experiment at 5 SLPM flow rate) is inserted and removed alternately for four times in the calibration system at 5 SLPM flow rate. The overall transmission efficiency of the system is shown in Fig. 4. The filter loss of the Teflon membrane (used for 2 h during the field experiment) is $10\pm3\%$ (Fig. 4). However, the filter loss of the new Teflon membrane filter is approximately $8\pm3\%$, as measured using the same calibration method. The results are similar with the results measured by Brown et al. [28]. The transmission efficiency difference between new membrane filter and used membrane filter (for about 2 h during the field experiment) is relatively small (approximately 2%), that causes no significant influence on accurate measurement of NO_3 radical under the situation of high particles concentration. In fact, the output of the heated N_2O_5 source tends to change over time. The NO_3 radical concentration from the output of heated N_2O_5 source gradually increases during the filter transmission measurement period (approximately 12 min). A linear fit depending on the time is implemented (R^2 larger than 0.99) for correcting NO_3 radical.

The loss rate of the NO_3 radical through the PFA tubing is $0.19\pm0.02\ s^{-1}$ and the filter loss of new Teflon membrane filter is approximately $8\pm3\%$. In addition, the surface loss of the filter holder is $9\pm4\%$. The overall inlet transmission efficiency of NO_3 radical for our instrument is $75\pm5\%$ at 5 SLPM flow rate (residence time of approximately 0.4 s).

4. Results and discussion

4.1. Effective absorption cross section

To get a better sensitivity of the instrument and avoid the interference of other species, the wavelength of the diode laser is chosen to be close to the largest absorption cross section of the NO_3 radical, where other trace gases should have the smallest absorption or no absorption. In addition, the wavelength of the diode laser must be stable to reduce uncertainty of the absorption cross section. During the continuous measurement of 8 h, the uncertainty of a wavelength is less than 0.01 nm by controlling the temperature. Besides, full width at half maximum (FWHM) of the diode laser is also considered, which should be significantly smaller than that of the NO_3 radical absorption width to ensure the measured ring-down decays in the presence of NO_3 radical as single exponential [42]. The center wavelength and FWHM of the diode laser are measured using a grating spectrometer (SR303i, Andor). The red solid line in Fig. 5 is the water vapor spectrum obtained from the HITRAN database [43]. To reduce the interference of water vapor, the wavelength of the diode laser is selected at the smaller absorption cross section of the water vapor. According to the above analysis, the center wavelength of the diode laser is selected at 661.85 nm with an FWHM of 0.3 nm by changing the temperature and external modulation of the diode laser (blue solid line in Fig. 5). Furthermore, the effective absorption cross section (shown in Fig. 5 as black solid line) is obtained by convolution of the laser spectrum and the absorption cross section of the NO_3 radical [44]. As a result, the NO_3 radical effective absorption cross section is $2.02\times10^{-17}\ cm^2\ molecule^{-1}$ for our instrument.

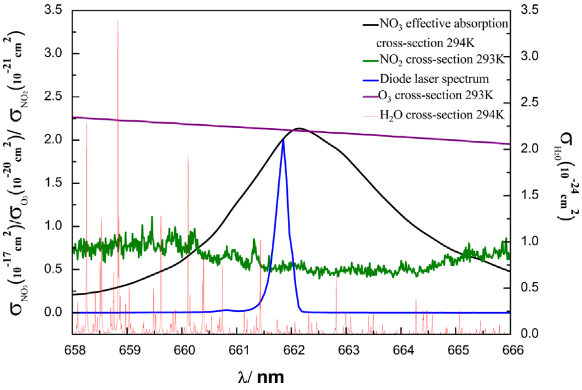

Fig. 5. Cross section of the NO_3 radical, NO_2, O_3, water vapor, and diode laser spectrum. (For interpretation of the references to color in this figure, the reader is referred to the web version of this article.)

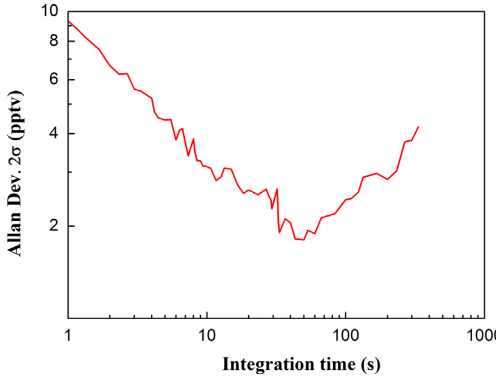

Fig. 6. Allan variance plot for the NO_3 radical measurements when sampling ambient air at daytime. The instrument has 2σ precision better than 3.2 pptv for a 10 s integration time.

4.2. Interference analysis

Mie scattering from atmospheric aerosol contributes to optical extinction in the cavity and leads to very large shot to shot fluctuations in τ_0, affecting the accurate measurement of NO_3 radical. Thus, the aerosol should be removed by the filter to reduce Mie scattering interference. In addition, to reduce the effect of Rayleigh scattering, the atmospheric pressure in the cavity must remain stable. In this case, Rayleigh scattering appears as a constant background, which limits the value of τ_0 but does not produce variability in τ_0. Variability of NO_2 and O_3, and water vapor in the atmosphere can produce spurious structure in the 661.85 nm absorption signal, which causes the interference of NO_3 radical measurements. Considering that the NO_3 radical cross section is larger (factor 9) than the water vapor cross section at 661.85 nm [43], this effect of the water vapor is relativity low. Once the ambient relative humidity changes to 10% (294 K), it causes an uncertainty of 1.26 pptv for the NO_3 radical. Each 1 ppbv of O_3 or NO_2 produces a baseline shift equivalent to 0.10 pptv and 0.27 pptv of NO_3 radical (293 K), respectively, based on their known absorption cross sections at 661.85 nm [45,46]. Changes in O_3, NO_2, water vapor, aerosol, and pressure in the atmosphere over time cause baseline shift; hence, τ_0 must be measured by NO titration every 3–5 min to reduce the interference of variability in the background.

4.3. Detection limit and accuracy

The minimum detection limit of the instrument can be presented as follows [27,47]:

$$[A]_{min} = \frac{R_L}{c\sigma}\frac{(\tau_0-\tau)_{min}}{\tau_0^2} \cong \frac{R_L}{c\sigma}\frac{\sqrt{2}\sigma(\tau_0)}{\tau_0^2} = \frac{R_L}{c\sigma}\frac{\sqrt{2}\delta\tau_0}{\tau_0} \quad (5)$$

where $[A]_{min}$ is the smallest measurable concentration and $(\tau_0-\tau)_{min}$ is the minimum measurable variation of ring down time. $(\tau_0-\tau)_{min}$ can be instead of the τ_0 standard deviation $\sigma(\tau_0)$. $\delta\tau_0$ is the fractional uncertainty of τ_0. For our instrument, τ_0 at 661.85 nm is roughly 68.00 μs and $\sigma(\tau_0)$ is approximately 0.065 μs for a 10 s integration time in the field measurement ($\sigma(\tau_0)$ is mainly affected by high particles and can achieve approximately 0.04 μs in the laboratory). Taking absorption cross section σ=2.02 × 10^{-17} cm^2 $molecule^{-1}$ for NO_3 radical at 661.85 nm (standard temperature and pressure), the detection limit of NO_3 radical is below 3.2 pptv (2σ) for a 10 s integration time. Fig. 6 shows the measurement of the NO_3 radical instrument baseline precision in the field when sampling ambient air at daytime.

Given that the interference between the inlet system flow and the dry N_2 mirror purges stream, R_L cannot be simply calculated by the ratio of the length between the two pieces of mirrors to that of the cavity inlet and outlet. For the CRDS system, we make use of the absorption of O_3 at 661.85 nm by flowing known concentrations of O_3 through the CRDS cell. Based on the known O_3 absorption cross section, R_L can be calculated using Eq. (1). The experimental results show that R_L is 1.196 ± 0.06.

For NO_3 radical measurements, the uncertainty of the NO_3 radical effective absorption cross-section is ±4% [48]. The uncertainty of the NO_3 radical effective absorption cross-section caused by the stability of the diode laser wavelength is 1.5%. Combining the uncertainty of R_L (±5%) and the uncertainty of the inlet transmission efficiency (±5%) yields the overall uncertainty in NO_3 radical of ±8% (1σ) for the CRDS system. The largest uncertainties of NO_3 radical caused by the baseline shift during the period of 3–5 min are approximately ±1.0 pptv (the variation of O_3, NO_2 and H_2O respectively estimated at ±2 ppbv, ±2 ppbv and ±2%).

4.4. Measurements of ambient NO_3 radical

The CRDS instrument for measuring NO_3 radical is deployed on the campus of University of Chinese Academy of Sciences, located in the northeast of Beijing, China. Measurements were performed from October 26 to November 11, 2014. The observation site is close to Jingjia national highway (G111), which is a busy highway with heavy traffic; thus, vehicles are the major source of emission in the vicinity and large amount of local NO is produced. In the case, NO_3 radical is only detectable occasionally. Fig. 7 shows the nighttime observation of NO_3 radical for the days that have relatively higher NO_3 radical mixing ratios from October 26 to November 11, 2014. The observed NO_3

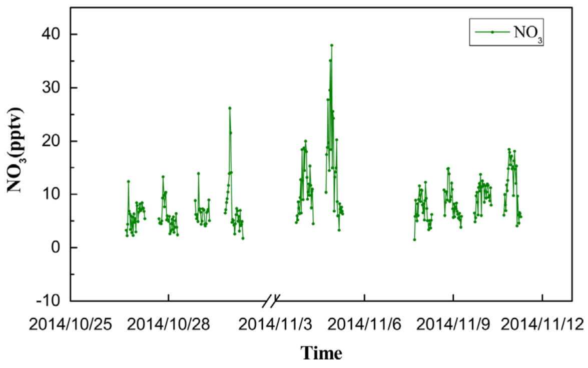

Fig. 7. NO_3 radical is observed by the CRDS instrument on the campus of Chinese Academy of Sciences University from October 26 to November 11, 2014. The mixing ratios of NO_3 radical are shown in the figure with the time resolution of 30 min.

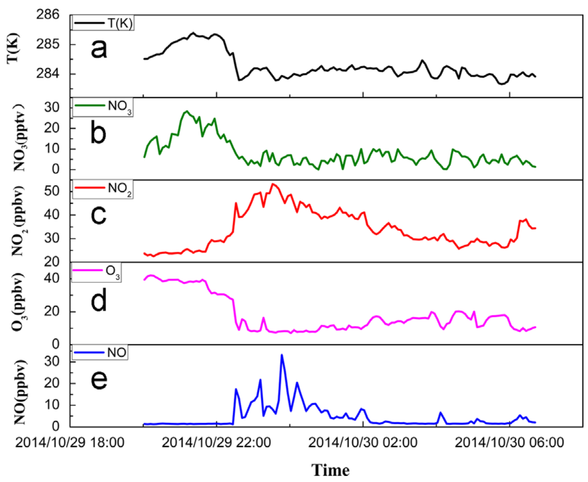

Fig. 8. NO_3, O_3, NO_2 and NO mixing ratios at 20:00 on October 29 to 7:00 on October 30, 2014. NO_3 radical mixing ratios are observed by the CRDS instrument. NO and NO_2 mixing ratios are measured by a nitrogen-oxide analyzer (Thermo Fisher 42i) with time resolution of 5 min. O_3 mixing ratios are measured by an ozone analyzer (Thermo Fisher 49i) with time resolution of 5 min.

radical mixing ratios vary from the minimum around the detection limit to 38 pptv. The NO_3 radical mixing ratios are higher (above 20 pptv) on October 29 and November 4, whereas relatively low for other days.

The nighttime observation of NO_3, O_3, NO_2 and NO from October 29 to October 30, 2014 is shown in Fig. 8. The mixing ratios of NO_3 radical rise rapidly from 6 pptv to 32 pptv from 20:26 to 22:30 on October 29, the highest value recorded in this period. In the meanwhile, O_3 reach to the higher mixing ratios of 40 ppbv and NO_2 mixing ratios are lower. The mixing ratios of NO are relatively small before 22:30, corresponding to the peak of NO_3 radical mixing ratios, while the mixing ratios of NO_3 radical and O_3 rapidly decrease as the mixing ratios of NO suddenly rising after 22:30. Thus, it is reasonable to assume that the increasing mixing ratios of NO (above 10 ppbv) are responsible for the removal of NO_3 radical and O_3. In addition, the inverse correlation between O_3 mixing ratios and NO_2 mixing ratios is found, and the increasing NO_2 may be caused by the reaction of NO and O_3.

5. Conclusions

In this study, we describe an instrument to detect atmospheric NO_3 radical by cavity ring-down spectroscopy. The detection limit for NO_3 radical is 3.2 pptv (2σ, 10 s) in the field with high particles and the instrument has the advantage of smaller power consumption, size, and weight. The surface loss and the membrane filter loss of NO_3 radical in the system are calibrated using synthetic N_2O_5 source. The experimental results show the overall transmission efficiency of the NO_3 radical at approximately $75 \pm 5\%$ at the flow rate of 5 SLPM.

Moreover, the measurement of NO_3 radical is performed on the campus of the University of Chinese Academy of Sciences from October 26 to November 11, 2014. According to the measurement results on October 29, the low NO_3 radical concentration is associated with the large amount of produced NO (above 10 ppbv). To our knowledge, this is the first time that a CRDS instrument is applied to detect atmospheric NO_3 radical in the suburb of Beijing, China under the situation of high particles concentration. The experimental results demonstrate the feasibility of CRDS to detect NO_3 radical under the situation of composite atmospheric pollution in China (high particles). Moreover, it will be further applied to research nocturnal atmospheric chemistry in China under the situation of high particles concentration.

Acknowledgments

This work was funded by the “Strategic Priority Research Program” of the Chinese Academy of Sciences (XDB05040200,XDB05010500), Key Research Program of the Chinese Academy of Sciences (KJZD-EW-TZ-G06-01) and National Natural Science Foundation of China (61108031, 41275038 and 41305139). Special thanks for the effective support of University of Chinese Academy of Sciences.

Appendix A. Supporting information

Supplementary data associated with this article can be found in the online version at http://dx.doi.org/10.1016/j.jqsrt.2015.07.005.

References

[1] Wayne RP, Barnes I, Biggs P, Burrows JP, Canosa-Mas CE, Hjorth J, et al. The nitrate radical: physics, chemistry and the atmosphere. Atmos Environ 1991;25A:1–206.
[2] Geyer A, Alicke B, Konrad S, Schmitz T, Stutz J, Platt U. Chemistry and oxidation capacity of the nitrate radical in the continental boundary layer near Berlin. J Geophys Res 2001;106:8013–25.
[3] Platt U, Alicke B, Dubois R, Geyer A, Hofzumahaus A, Holland F, et al. Free radicals and fast photochemistry during BERLIOZ. J Atmos Chem 2002;42:359–94.
[4] Atkinson R. Kinetics and mechanisms of the gas-phase reactions of the NO_3 radical with organic compounds. J Phys Chem Ref Data 1991;20:459–507.

[5] Brown SS, Stutz J. Nighttime radical observations and chemistry. Chem Soc Rev 2012;41:6405–47.

[6] Jones CL, Seinfeld JH. The oxidation of NO_2 to nitrate—day and night. Atmos Environ 1983;17:2370–3.

[7] Atkinson R, Baulch DL, Cox RA, Crowley JN, Hampson RF, Hynes RG, et al. Evaluated kinetic and photochemical data for atmospheric chemistry: volume I – gas phase reactions of O-*x*, HO*x*, NO*x* and SO*x* species. Atmos Chem Phys 2004;4:1461–738.

[8] Platt U, Perner D, Winer AM, Harris GW, Pitts JN. Detection of NO_3 in the polluted troposphere by differential optical-absorption. Geophys Res Lett 1980;7:89–92.

[9] Allan BJ, Carslaw N, Coe H, et al. Observations of the nitrate radical in the marine boundary layer. J Atmos Chem 1999;33:129–54.

[10] Plane JMC, Nien C. Differential optical-absorption spectrometer for measuring for measuring atmospheric trace gases. Rev Sci Instrum 1992;63:1867–76.

[11] Heintz F, Platt U, Flentje H, Dubois R. Long-term observation of nitrate radicals at the tor station, Kap Arkona (Rugen). J Geophys Res 1996;101:22891–910.

[12] Asaf D, Pedersen D, Matveev V, Peleg M, Kern C, Zingler J, et al. Long-term measurements of NO_3 radical at a semiarid urban site: 1. Extreme concentration events and their oxidation capacity. Environ Sci Technol 2009;43:9117–23.

[13] McLaren R, Wojtal P, Majonis D, McCourt J, Halla JD, Brook J. NO_3 radical measurements in a polluted marine environment: links to ozone formation. Atmos Chem Phys 2010;10:4187–206.

[14] Li SW, Liu WQ, Xie PH, Qin M, Yang YJ. Observation of nitrate radical in the nocturnal boundary layer during a summer field campaign in Pearl River Delta, China. Terr Atmos Ocean Sci 2012;23:39–48.

[15] Wang SS, Shi CZ, Zhou B, Zhao H, Wang ZR, Yang SN, et al. Observation of NO_3 radicals over Shanghai, China. Atmos Environ 2013;70:401–9.

[16] Wagner NL, Dubé WP, Washenfelder RA, Young CJ, Pollack IB, Ryerson TB, et al. Diode laser-based cavity ring-down instrument for NO_3, N_2O_5, NO, NO_2 and O_3 from aircraft. Atmos Meas Tech 2011;4:1227–40.

[17] Wu T, Coeur-Tourneur C, Dhont G, Cassez A, Fertein E, He XD, et al. Simultaneous monitoring of temporal profiles of NO_3, NO_2 and O-3 by incoherent broadband cavity enhanced absorption spectroscopy for atmospheric applications. J Quant Spectrosc Radiat Transf 2014;133:199–205.

[18] Zheng J, Zhang R, Fortner EC, Volkamer RM, Molina L, Aiken AC, et al. Measurements of HNO_3 and N_2O_5 using ion drift-chemical ionization mass spectrometry during the MILAGRO/MCMA-2006 campaign. Atmos Chem Phys 2008;8:6823–38.

[19] Dorn HP, Apodaca RL, Ball SM, Brauers T, Brown SS, Crowley JN, et al. Intercomparison of NO_3 radical detection instruments in the atmosphere simulation chamber SAPHIR. Atmos Meas Tech 2013;6:1111–40.

[20] Slusher DL, Huey LG, Tanner DJ, Flocke F, Roberts JM. A thermal dissociation—chemical ionization mass spectrometry (TD-CIMS) technique for the simultaneous measurement of peroxyacetyl radicals and dinitrogen pentoxide. J Geophys Res 2004;109:D19315.

[21] Wang X, Wang T, Yan C, Tham YJ, Xue L, Xu Z, et al. Large daytime signals of N_2O_5 and NO_3 inferred at 62 amu in a TD-CIMS: chemical interference or a real atmospheric phenomenon? Atmos Meas Tech 2014;7:1–12.

[22] Varma RM, Venables DS, Ruth AA, Heitmann U, Schlosser E, Dixneuf S. Long optical cavities for open-path monitoring of atmospheric trace gases and aerosol extinction. Appl Opt 2009;48:B150–71.

[23] Kennedy OJ, Ouyang B, Langridge JM, Daniels MJS, Bauguitte S, Freshwater R, et al. An aircraft based three channel broadband cavity enhanced absorption spectrometer for simultaneous measurements of NO_3, N_2O_5 and NO_2. Atmos Meas Tech 2011;4:1759–76.

[24] Venables DS, Gherman T, Orphal J, Wenger JC, Ruth AA. High sensitivity in situ monitoring of NO_3 in an atmospheric simulation chamber using incoherent broadband cavity enhanced absorption spectroscopy. Environ Sci Technol 2006;40:6758–63.

[25] Langridge JM, Ball SM, Shillings AJL, Jones RL. A broadband absorption spectrometer using light emitting diodes for ultrasensitive, in situ trace gas detection. Rev Sci Instrum 2008;79:123110.

[26] Brown SS, Stark H, Ciciora SJ, Ravishankara AR. In-situ measurement of atmospheric NO_3 and N_2O_5 via cavity ring-down spectroscopy. Geophys Res Lett 2001;28:3227–30.

[27] Brown SS, Stark H, Ciciora SJ, McLaughlin RJ, Ravishankara AR. Simultaneous in situ detection of atmospheric NO_3 and N_2O_5 via cavity ring-down spectroscopy. Rev Sci Instrum 2002;73:3291–301.

[28] Dubé WP, Brown SS, Osthoff HD, Nunley MR, Ciciora SJ, Paris MW, et al. Aircraft instrument for simultaneous in situ measurement of NO_3 and N_2O_5 via pulsed cavity ring-down spectroscopy. Rev Sci Instrum 2006;77:034101.

[29] Fuchs H, Dubé WP, Ciciora SJ, Brown SS. Determination of inlet transmission and conversion efficiencies for in situ measurements of the nocturnal nitrogen oxides, NO_3, N_2O_5 and NO_2, via pulsed cavity ring-down spectroscopy. Anal Chem 2008;80:6010–7.

[30] Ayers JD, Apodaca RL, Simpson WR, Baer DS. Off-axis cavity ring-down spectroscopy: application to atmospheric nitrate radical detection. Appl Opt 2005;44:7239–42.

[31] Schuster G, Labazan I, Crowley JN. A cavity ring down/cavity enhanced absorption device for measurement of ambient NO_3 and N_2O_5. Atmos Meas Tech 2009;2:1–13.

[32] Brown SS, Dubé WP, Osthoff HD, Wolfe DE, Angevine WM, Ravishankara AR. High resolution vertical distributions of NO_3 and N_2O_5 through the nocturnal boundary layer. Atmos Chem Phys 2007;7:139–49.

[33] Brown SS, Dibb JE, Stark H, Aldener M, Vozella M, Whitlow S. Nighttime removal of NO*x* in the summer marine boundary layer. Geophys Res Lett 2004;31:L07108.

[34] Crowley JN, Thieser J, Tang MJ, Schuster G, Bozem H, Beygi ZH, et al. Variable lifetimes and loss mechanisms for NO_3 and N_2O_5 during the DOMINO campaign: contrasts between marine, urban and continental air. Atmos Chem Phys 2011;11:10853–70.

[35] O'Keefe A, Deacon DAG. Cavity ring-down optical spectrometer for absorption measurements using pulsed laser sources. Rev Sci Instrum 1988;59:2544–51.

[36] Scherer JJ, Paul JB, Okeefe A, Saykally RJ. Cavity ring down laser absorption spectroscopy: history, development, and application to pulsed molecular beams. Chem Rev 1997;97:25–51.

[37] Wheeler MD, Newman SM, Orr-Ewing AJ, Ashfold MNR. Cavity ring-down spectroscopy. J Chem Soc Faraday Trans 1998;94:337–51.

[38] Wang LM, Zhang JS. Detection of nitrous acid by cavity ring down spectroscopy. Environ Sci Technol 2000;34:4221–7.

[39] Everest Michael A, Atkinson DB. Discrete sums for the rapid determination of exponential decay constants. Rev Sci Instrum 2008;79:023108.

[40] Wand D, Xie PH, Hu RZ, Qin M, Ling LY, Duan J. Fast and accurate extraction of ring- down time in cavity ring-down spectroscopy. Spectrosc Spectr Anal 2014;34:2845–50.

[41] Davidson JA, Viggiano AA, Howard CJ, Dotan I, Fehsenfeld FC, Albritton DL, et al. Rate constants for reactions of O_2^+, NO_2^+, NO^+, H_3O^+, CO_3^-, NO_2^-, and halide ions with N_2O_5 at 300 K. J Chem Phys 1978;68:2085–7.

[42] Zalicki P, Zare RN. Cavity ring-down spectroscopy for quantitative absorption-measurements. J Chem Phys 1995;102:2708–17.

[43] Rothman LS, Gordon IE, Babikov Y, Barbe A, Benner DC, Bernath PE, et al. The HITRAN2012 molecular spectroscopic database. J Quant Spectrosc Radiat Transf 2013;130:4–50.

[44] Orphal J, Fellows CE, Flaud PM. The visible absorption spectrum of NO_3 measured by high-resolution Fourier transform spectroscopy. J Geophys Res 2003;108:4077–87.

[45] Voigt S, Orphal J, Bogumil K, Burrows JP. The temperature dependence (203–293 K) of the absorption cross sections of O-3 in the 230–850 nm region measured by Fourier-transform spectroscopy. J Photochem Photobiol 2001;143:1–9.

[46] Voigt S, Orphal J, Burrows JP. The temperature and pressure dependence of the absorption cross-sections of NO_2 in the 250–800 nm region measured by Fourier-transform spectroscopy. J Photochem Photobiol 2002;149:1–7.

[47] Odame-ankrah Charles A, Hans D. Compact diode laser cavity ring-down spectrometer for atmospheric measurements of NO_3 and N_2O_5 with automated zeroing and calibration. Appl Spectrosc 2011;65:1260–8.

[48] Osthoff HD, Pilling MJ, Ravishankara AR, Brown SS. Temperature dependence of the NO(3) absorption cross-section above 298 K and determination of the equilibrium constant for NO(3)+NO(2)↔N(2)O(5) at atmospherically relevant conditions. Phys Chem Chem Phys 2007;9:5785–93.